Analytical and Bioanalytical Chemistry
https://doi.org/10.1007/s00216-023-04677-9

RESEARCH PAPER

Pilot investigation of magnetic nanoparticle–based immobilized metal affinity chromatography for efficient enrichment of phosphoproteoforms for mass spectrometry–based top-down proteomics

Qianyi Wang[1] · Fei Fang[1] · Liangliang Sun[1]

Received: 20 December 2022 / Revised: 23 March 2023 / Accepted: 28 March 2023

Abstract
Protein phosphorylation is a vital and common post-translational modification (PTM) in cells, modulating various biological processes and diseases. Comprehensive top-down proteomics of phosphorylated proteoforms (phosphoproteoforms) in cells and tissues is essential for a better understanding of the roles of protein phosphorylation in fundamental biological processes and diseases. Mass spectrometry (MS)–based top-down proteomics of phosphoproteoforms remains challenging due to their relatively low abundance. Herein, we investigated magnetic nanoparticle–based immobilized metal affinity chromatography (IMAC, Ti^{4+}, and Fe^{3+}) for selective enrichment of phosphoproteoforms for MS-based top-down proteomics. The IMAC method achieved reproducible and highly efficient enrichment of phosphoproteoforms from simple and complex protein mixtures. It outperformed one commercial phosphoprotein enrichment kit regarding the capture efficiency and recovery of phosphoproteins. Reversed-phase liquid chromatography (RPLC)–tandem mass spectrometry (MS/MS) analyses of yeast cell lysates after IMAC (Ti^{4+} or Fe^{3+}) enrichment produced roughly 100% more phosphoproteoform identifications compared to without IMAC enrichment. Importantly, the phosphoproteoforms identified after Ti^{4+}-IMAC or Fe^{3+}-IMAC enrichment correspond to proteins with much lower overall abundance compared to that identified without the IMAC treatment. We also revealed that Ti^{4+}-IMAC and Fe^{3+}-IMAC could enrich different pools of phosphoproteoforms from complex proteomes and the combination of those two methods will be useful for further improving the phosphoproteoform coverage from complex samples. The results clearly demonstrate the value of our magnetic nanoparticle–based Ti^{4+}-IMAC and Fe^{3+}-IMAC for advancing top-down MS characterization of phosphoproteoforms in complex biological systems.

Keywords Top-down proteomics · Phosphoproteoform · Immobilized metal affinity chromatography · Magnetic nanoparticle · RPLC-MS/MS

Introduction

Protein phosphorylation is a vital and common post-translational modification (PTM), modulating various biological processes and diseases [1–5]. Mass spectrometry (MS)–based phosphoproteomics has been widely deployed for large-scale characterization of protein phosphorylation in cells and tissues across various biological conditions [6]. However, almost all the phosphoproteomics studies were performed using bottom-up proteomics (BUP) [6], which cannot provide clear knowledge of phosphoprotein's proteoforms due to enzymatic digestion. Proteoforms are a group of protein molecules that derive from the same gene due to RNA alternative splicing and protein PTMs [7]. Strong pieces of evidence suggest that proteoforms from the same gene can have drastically different biological functions [8–11]. Therefore, the characterization of phosphoproteins in a proteoform-specific manner (i.e., phosphoproteoform) is critical for accurate understanding of phosphoproteins' biological function in biological processes and diseases [12].

Published in the topical collection *Young Investigators in (Bio-) Analytical Chemistry 2023* with guest editors Zhi-Yuan Gu, Beatriz Jurado-Sánchez, Thomas H. Linz, Leandro Wang Hantao, Nongnoot Wongkaew, and Peng Wu.

✉ Liangliang Sun
lsun@chemistry.msu.edu

[1] Department of Chemistry, Michigan State University, 578 S Shaw Lane, East Lansing, MI 48824, USA

Published online: 05 April 2023

Top-down proteomics (TDP), unlike BUP, characterizes intact proteoforms using mass spectrometry (MS) and tandem mass spectrometry (MS/MS), providing rich information on PTMs and their combinations on proteins [13]. TDP has been employed for large-scale identification and quantification of proteoforms across cells and tissues to better our understanding of fundamental biological processes and to determine disease-related proteoform biomarkers [12–19]. However, the TDP study of phosphoproteoforms has largely lagged behind because of the relatively low abundance of phosphoproteoforms in complex proteomes. It is also more challenging to enrich phosphoproteoforms compared to phosphopeptides due to their much larger size and much more complex structure than phosphopeptides. To advance the TDP of phosphoproteoforms, highly efficient and selective enrichment technologies for phosphoproteoforms are crucial.

A variety of techniques have been developed for the enrichment of phosphopeptides from complex peptide mixtures for BUP-based phosphoproteomics [6], including the most widely used immobilized metal affinity chromatography (IMAC, e.g., Ti^{4+} and Fe^{3+}) [20–23], antibody [24–26], ion exchange chromatography (IEX) [27, 28], and affinity tag [29, 30]. However, only a few studies investigated techniques for highly selective phosphoproteoform isolation for TDP. The Ge group synthesized several different novel nanoparticles with affinity tags for the enrichment of phosphoproteoforms from complex samples, followed by liquid chromatography–tandem mass spectrometry (LC–MS/MS)–based TDP analysis [31–33]. The Yu group synthesized a Ti^{4+}-IMAC material based on polyoxometalate (P_5W_{30})/polydopamine (PDA) composite microspheres for selective isolation of phosphoproteins, and SDS-PAGE was utilized to evaluate the performance of the IMAC for standard phosphoproteins and low-complexity samples [34]. Those studies have demonstrated the potential of large-scale top-down characterization of phosphoproteoforms with the assistance of selective enrichment techniques. However, much more efforts need to be made to achieve comprehensive TDP of phosphoproteome in a proteoform-specific manner regarding phosphoproteoform enrichment, separation, MS/MS, and identification through bioinformatic tools.

Herein, we investigated the magnetic nanoparticle–based IMAC materials with Ti^{4+} and Fe^{3+} for highly specific phosphoproteoform enrichment from a complex cell lysate for TDP for the first time. The IMAC procedure is similar to the typical one using IMAC for phosphopeptides but with substantially different buffers. The Ti^{4+}-IMAC and Fe^{3+}-IMAC magnetic materials were prepared using a well-established procedure with a relatively new linker for the immobilization of Ti^{4+} and Fe^{3+}. We systematically characterized the magnetic IMAC nanomaterials and evaluated its performance for phosphoproteoform enrichment using SDS-PAGE and LC–MS/MS. We compared the Ti^{4+}-IMAC and Fe^{3+}-IMAC methods regarding the identified phosphoproteoforms.

Materials and methods

Materials and reagents

All materials are purchased from Sigma-Aldrich (St. Louis, MO) unless otherwise stated. Amine-terminated nanoparticles were purchased from Polysciences (Warrington, PA). Sodium phosphate monobasic (NaH_2PO_4) and sodium cyanoborohydride ($NaBH_3CN$) were ordered from Fisher Scientific (Pittsburgh, PA). Pierce™ Phosphoprotein Enrichment Kit, Coomassie Brilliant Blue G-250, Pro-Q™ Diamond Phosphoprotein Gel Stain, and SYPRO™ Ruby Protein Gel Stain were purchased from Thermo Scientific (Waltham, MA). Mini-PROTEAN Precast Mini PAGE Gel was from Bio-rad (Hercules, CA). Tris, HEPES, sodium phosphate dibasic (Na_2HPO_4), and sodium chloride (NaCl) were ordered from Invitrogen (Waltham, MA), GoldBio (St. Louis, MO), Jade Scientific (Westland, MI), and ChemPure Brand (Westland, MI), respectively.

Preparation of Ti^{4+}-IMAC magnetic nanoparticles

The Ti^{4+}-IMAC nanoparticles were synthesized using commercially available reagents following the schematics shown in Fig. 1A. (1) Amine-terminated magnetic nanoparticles (10 mg) were suspended in 200 µL of deionized water. Water was removed by a magnet for isolation. Then, 600 µL of 10% (v/v) glutaraldehyde in 100 mM phosphate aqueous buffer (93.5 mM Na_2HPO_4, 6.5 mM NaH_2PO_4, pH 8.0) was added and mixed well with the nanoparticles via vortex for 10 s. Then, the mixture was kept at room temperature for 6 h under a gentle mixing condition with a tube revolver rotator (Thermo Scientific) at 15 rpm. After the reaction, the aldehyde-functionalized nanoparticles (Intermediate 1) were washed three times with 100 mM phosphate aqueous buffer (600 µL each time). (2) 600 µL of AMPA (aminomethylphosphonic acid, 2 mg/mL) and $NaBH_3CN$ (10 mg/mL) in 100 mM phosphate aqueous buffer was added to the Intermediate 1 for reaction at room temperature for 6 h under the same mixing condition as step 1. The Intermediate 2 was washed three times with LC–MS water. (3) 1.8 mL of 100 mM $TiCl_4$ in LC–MS water (note: precipitates were removed from the solution after mixing $TiCl_4$ with the water) was added to the Intermediate 2 for reaction at room temperature for 6 h under the same mixing condition as the previous steps to produce the final product, Ti^{4+}-IMAC magnetic nanoparticles. After washing with LC–MS water three times, the final product was kept in 200 µL of LC–MS water at 4 °C before use.

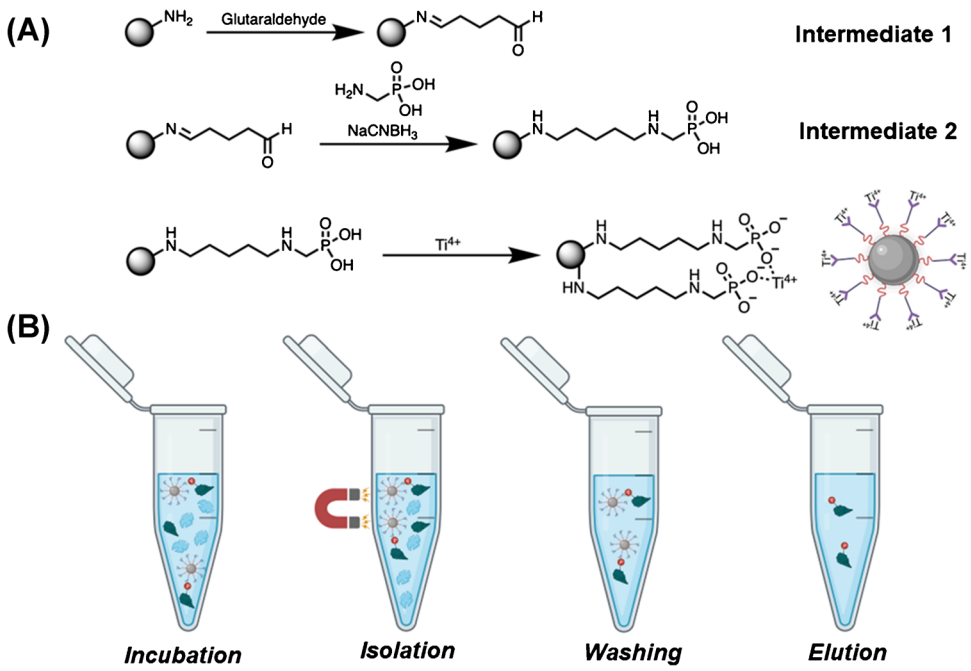

Fig. 1 **A** Schematic of the synthesis process of Ti^{4+}-IMAC magnetic nanoparticles. The Ti^{4+} chelated on the linker has strong binding to the phosphate groups. The cartoon at the bottom right shows the schematic diagram of the final product of Ti^{4+}-IMAC magnetic nanoparticles. **B** Schematic of the phosphoproteoform enrichment process from protein mixtures using magnetic nanoparticle–based Ti^{4+}-IMAC

Characterization of Ti^{4+}-IMAC magnetic nanoparticles

Transmission electron microscopy (TEM) was conducted on a JEOL JEM-1400 Flash instrument operated at 80 kV. Energy dispersive X-ray microanalysis (EDS) was carried out at 10 kV by an ultra-high resolution JEOL 7500F scanning electron microscope equipped with Oxford EDS systems for elemental analysis. Zeta potential was measured using the Zetasizer Nano instrument (Malvern Panalytical) at 377.6 kcps count rates, 12 zeta runs, 2.00 mm measurement position, and 5 attenuators. Thermogravimetric analysis (TGA) was conducted using a TGA Q500 thermal analysis system (Waters Corporation) under a N_2 atmosphere at a constant heating rate of 10 °C/min from 100 to 600 °C. All samples were first heated to 100 °C and held at that temperature for 2 min to fully dry down the particles.

Phosphoprotein enrichment using Ti^{4+}-IMAC magnetic nanoparticles and the commercial kit: standard proteins

The procedure for phosphoprotein enrichment with the Ti^{4+}-IMAC is shown in Fig. 1B. A mixture of bovine serum albumin (BSA, unphosphorylated protein) and β-casein (phosphorylated protein) was dissolved in the loading buffer (50 mM HEPES–NaOH, 200 mM NaCl, pH 7.0). Then, the sample (4.5 mL) was mixed with Ti^{4+}-IMAC nanoparticles (10 mg) and kept at room temperature for 2 h. Next, the nanoparticles were washed twice with the loading buffer (4.5 mL) to remove non-specific binding proteins. At last, the phosphoproteins bound to the nanoparticles were eluted twice with about 2 mL of elution buffer (200 mM Na_2HPO_4, 200 mM NaCl, pH 7.0). The two eluates were combined. Protein concentration in the loading mixture (LM), flow-through (FT), and elution (E) samples was measured by the bicinchoninic acid (BCA) assay. These samples were mixed with a 4X SDS-PAGE sample buffer (1.0 M Tris pH 6.8, 2 mL; SDS, 0.8 g; Bromophenol Blue, 0.04 g; Glycerol, 4 mL; LC/MS grade water, 4 mL; 1 M DTT, 1 mL), and boiled at 94 °C for 10 min. Then, a Mini-PROTEAN Precast Mini PAGE Gel (Bio-rad) was used for gel electrophoresis. The parameters for SDS-PAGE were set at 150 V for 50 min. After Coomassie Blue staining, the recovery rate was calculated using the ImageJ software (*%Recovery = amount of β-casein after enrichment/amount of β-casein before enrichment × 100%*).

For the phosphoprotein enrichment using the commercial kit, the Pierce™ phosphoprotein enrichment kit was used following the manufacturer's protocol. First, the storage solution was removed, and 5 mL of the loading buffer was applied to equilibrate the commercial column via centrifugation at 1000 × g for 1 min at 4 °C. Second, 4 mg of the standard protein mixture (BSA, 10 µM; β-casein, 10 µM) in the loading buffer (LM) was incubated with the column on a tube revolver rotator for 30 min at 4 °C. Third, the flow-through (FT) was collected by centrifugation at 1000 × g for 1 min at 4 °C. Fourth, the column was washed three times with 4.5 mL loading buffer in total via centrifugation at 1000 × g for 1 min at 4 °C to remove the non-specific protein binding (W1, W2, and W3). Finally, the phosphoproteins were eluted four times using a total volume of 4.5 mL

elution buffer (E) via centrifugation at 1,000 × g for 1 min at 4 °C. The eluted sample was desalted and concentrated to 1 mL for SDS-PAGE analysis as described above.

Preparation of yeast cell lysate, phosphoproteoform enrichment, and SDS-PAGE analysis

The baker's yeast (YSC1 purchased from Sigma-Aldrich) was cultured in YPD broth (Sigma-Aldrich) according to the general yeast growth protocol. After the harvest, the yeast was washed 3 times by the loading buffer and well dispersed in the loading buffer supplemented with 1 × cOmplete protease inhibitor and 1 × PhosSTOP phosphatase inhibitor. The yeast was lysed for 2 min using a homogenizer 150 (Fisher Scientific) and then sonicated on ice for 10 min by a Branson Sonifier 250 (VWR Scientific). Next, the yeast lysate was centrifuged at 14,000 g for 10 min under 4 °C. The supernatant was kept, and the protein concentration was measured by the BCA assay. The extracted proteins were stored at − 80 °C before use.

The phosphoproteoform enrichment procedure was the same as the standard protein mixture experiment (BSA and β-casein) with some modifications. Yeast proteins measuring 3 mg in 1 mL loading buffer were mixed with 10 mg of IMAC magnetic nanoparticles. A loading buffer measuring 1 mL was used for washing the beads twice to remove non-specific binding. An elution buffer measuring 200 µL was used to elute phosphoproteoform from beads twice. After enrichment, the loading mixture (LM), flow-through (FT), and elution (E) were desalted with a 10-kDa molecular weight cutoff membrane (Millipore Sigma, Inc) before analysis.

Yeast proteins of LM, FT, and E measuring 15 µg were separated by SDS-PAGE. Precast Mini PAGE Gel (4–20%, Bio-rad) was used for gel electrophoresis (150 V, 50 min). The gel was stained with Pro-Q™ Diamond Phosphoprotein Gel Stain followed by SYPRO™ Ruby Protein Gel Stain according to the manufacturers' protocols. To visualize phosphoproteins and all the proteins, the gel was imaged using a ChemiDoc MP system (Bio-rad) with built-in settings for Pro-Q Diamond and SYPRO Ruby fluorescent dye separately.

Phosphoproteoform enrichment from yeast cell lysate and reversed-phase LC (RPLC)-MS/MS

The phosphoproteoform enrichment procedure was the same as mentioned before except that 5 mg of yeast proteins was used as the starting material. About 200 µg of proteins was recovered in the eluate (E) after the enrichment. The protein sample was dissolved in 400 µL of 0.1% (v/v) formic acid (0.5 mg/mL).

For RPLC-MS/MS, an EASY-RPLC™ 1200 system and a Q-Exactive HF mass spectrometer (Thermo Fisher Scientific) (Thermo Fisher Scientific) were used. The yeast sample was dissolved in 0.1% (v/v) FA. One microliter of the sample corresponding to 0.5 µg proteins was separated on a home-packed C4 separation column (100-µm i.d. × 30 cm, 3 µm particles, 300 Å, Sepax Technologies, Inc.) at a flow rate of 500 nL/min. Mobile phase A was 5% (v/v) ACN in water containing 0.1% (v/v) FA), and mobile phase B was 80% (v/v) ACN and 0.1% (v/v) FA. For separation, a 105-min gradient was used: 0–85 min, 5–70% B; 85–90 min, 70–100% B; 90–105 min, 100% B.

The electrospray voltage was set to 1.8 kV. A Top5 DDA method was used. The mass resolution was set to 120,000 (at *m/z* 200) for full MS scans and 60,000 (at *m/z* 200) for MS/MS scans. For full MS scans and MS/MS scans, the target value was 3E6 and 1E6; the maximum injection time was 100 ms and 200 ms, respectively. The scan range was 600 to 2000 m/*z* for full MS scans. For MS/MS scans, the isolation window was 4 m/*z*. Fragmentation in the HCD cell was performed with a normalized collision energy of 20%. The fixed first mass was set to 100 m/*z* for MS/MS. Dynamic exclusion was applied and it was set to 30 s. Ions with charge states from + 1 to + 5 were not considered for fragmentation.

Data analysis

All the RAW files were analyzed with the TopPIC (top-down mass spectrometry–based proteoform identification and characterization) software (version 1.5.2) [35].

The RAW files were first converted to mzML files with the MsConvert software [36], and spectral deconvolution was performed with the TopFD (top-down mass spectrometry feature detection) software, generating msalign files, which were used as the input for database searching using TopPIC. The spectra were searched against a yeast database (downloaded from Swiss-Uniprot, September 2021). False discovery rates (FDRs) were estimated using the target-decoy approach [37, 38]. A 1% proteoform spectrum match (PrSM)-level FDR and a 5% proteoform-level FDR were employed to filter the identifications. The mass error tolerance was 15 ppm. The mass error tolerance was 1.2 Da for identifying PrSM clusters. The maximum mass shift was 500 Da. The maximum number of mass shifts was set to 2.

For phosphoproteoform determination, we used multiple strategies. First, we manually checked the reported mass shifts from TopPIC, considering single phosphorylation (around 80-Da mass shift), multiple phosphorylation (i.e., around 160-Da and 240-Da mass shifts), and combinations of phosphorylation and other common PTMs (e.g., methylation and acetylation). Second, we confirmed those PTMs according to the information on UniProt database (https://www.uniprot.org) and YAAM database (http://yaam.ifc.unam.mx). Third, we manually checked the MS/MS spectra of some identified phosphoproteoforms for the neutral loss of phosphorylation (80-Da or 98-Da) caused by HCD fragmentation.

Results and discussion

Characterization of Ti^{4+}-IMAC magnetic nanoparticles

The synthesis of Ti^{4+}-IMAC nanoparticles is shown in Fig. 1A. First, the amine-terminated nanoparticles (ATNPs) were mixed with glutaraldehyde to bring an aldehyde group to the NPs. Then, this intermediate 1 reacted with sodium cyanoborohydride and AMPA to generate stable phosphate groups to the NPs. Finally, the Ti^{4+} was immobilized on the surface of intermediate 2 based on the chelating interaction between the phosphate group and Ti^{4+}.

The TEM results (Fig. 2A) revealed the size of the Ti^{4+}-IMAC magnetic nanoparticles is smaller than 20 nm, and the functionalization did not increase the particle size compared to the initial ATNPs, most likely because the reactions only added short carbon chains to the particle surface. Figure 2B shows the elemental composition analysis data of ATNPs and Ti^{4+}-IMAC nanoparticles from EDS. Ti^{4+}-IMAC nanoparticles had substantially higher amounts of Ti^{4+} and P compared to ATNPs (Ti^{4+}, 8.5% vs. 0%; P, 4.7% vs. 0%), indicating the successful functionalization of the magnetic nanoparticles with phosphate groups and Ti^{4+} ions. Additionally, we further characterized the zeta potentials of ATNPs and Ti^{4+}-IMAC nanoparticles by laser Doppler velocimetry (LDV) (Fig. 2C). The zeta potential of the ATNPs and Ti^{4+}-IMAC nanoparticles were 19.8 mV and – 29.6 mV. This negative shift is due to the replacement of the amine group to the phosphate group on the nanoparticle surface. Finally, the TGA analysis results of ATNPs and Ti^{4+}-IMAC nanoparticles demonstrated a much more significant weight loss of Ti^{4+}-IMAC compared to the original ATNPs (Fig. 2D). The phenomenon is due to several more chemical modifications of the Ti^{4+}-IMAC nanoparticles compared to the original ATNPs. Figure 2E shows that the Ti^{4+}-IMAC magnetic particles can be well dispersed in water and easily separated from water by a magnet, which guarantees efficient interactions between nanoparticles and phosphoproteins as well as easy operations.

Phosphoprotein enrichment by the Ti^{4+}-IMAC nanoparticles and SDS-PAGE analysis: standard proteins

We used a standard protein mixture containing β-casein (β, a phosphoprotein) and bovine serum albumin (BSA, a non-phosphoprotein) to evaluate the performance of Ti^{4+}-IMAC nanoparticles for selectively isolating phosphoproteins. The experimental procedure is shown in Fig. 1B, including (1) mixing and incubating the protein mixture (loading mixture, LM)

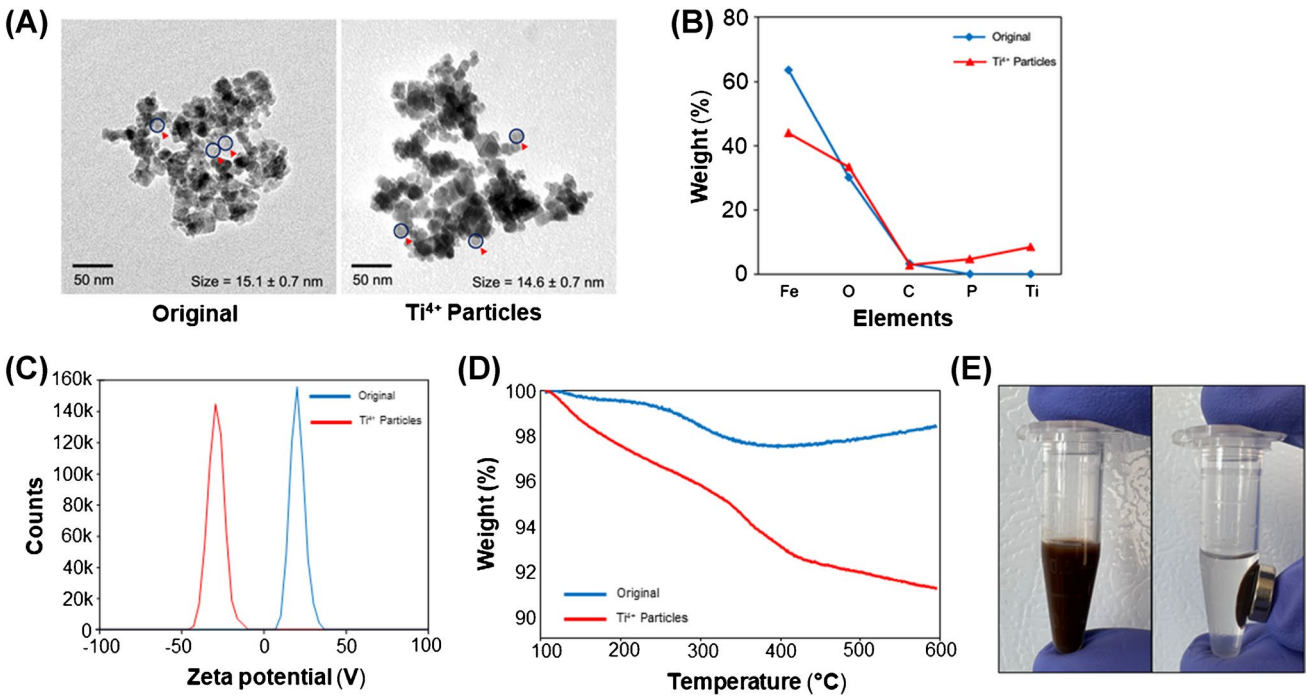

Fig. 2 Characterization results of magnetic nanoparticle–based Ti^{4+}-IMAC material, including TEM (**A**), elemental composition analysis (**B**), zeta potential analysis (**C**), weight loss analysis (**D**), and water dispersion and magnetic separation tests (**E**). Each red arrow in **A** is pointing at a single magnetic nanoparticle and those nanoparticles were used to estimate the means and standard deviations of the size of original ATNPs and Ti^{4+}-IMAC nanoparticles

with the Ti^{4+}-IMAC, (2) selectively isolating the phosphoproteins by the Ti^{4+}-IMAC and removing the non-phosphoproteins in the solution (flow-through, FT), (3) washing away the non-phosphoproteins efficiently by a couple of washing steps (Wash 1 and 2, W1 and W2), and (4) eluting phosphoproteins from the Ti^{4+}-IMAC (elution, E). We chose the salt concentrations in the loading buffer, washing buffer, and elution buffer according to one previous report. [31] We optimized the pH of the loading buffer, washing buffer, and elution buffer using the standard protein mixture (BSA and β-casein molar ratio as 10:1, 100 μM:10 μM); see Electronic Supplementary Material I Figure S1. We used SDS-PAGE to evaluate the enrichment efficiency of phosphoproteins, and the gel was stained with Coomassie Blue dye to observe the phosphoproteins and non-phosphoproteins. After considering both non-phosphoprotein removal and phosphoprotein recovery, we decided to choose the pH 7.0 buffers for all the following experiments. The loading and washing buffer contained 50 mM HEPES–NaOH and 200 mM NaCl (pH 7.0). The elution buffer contained 200 mM NaCl and 200 mM Na_2HPO_4 (pH 7.0).

Figure 3 shows the SDS-PAGE data of the standard protein mixture (1:1 molar ratio of BSA: β-casein, 10 μM:10 μM) after treatment by the Ti^{4+}-IMAC (A) and the commercial kit (B) as well as the standard protein mixture (10:1 molar ratio of BSA: β-casein, 100 μM:10 μM) after treatment by the Ti^{4+}-IMAC (C). It is clear that Ti^{4+}-IMAC can selectively capture the phosphoprotein (β-casein) and efficiently remove the non-phosphoprotein (BSA) even when BSA has a ten-fold higher concentration than β-casein (Fig. 3A and C). Compared to the commercial kit (Fig. 3B), the Ti^{4+}-IMAC had a better performance regarding the capture efficiency for phosphoproteins. As marked by the red ovals, clear β-casein bands were observed in the flow-through (FT) and Wash (W1) samples from the commercial kit; no obvious signals were obtained in FT and W1 samples from the Ti^{4+}-IMAC. The β-casein recovery from the Ti^{4+}-IMAC is much higher than that from the commercial kit (46% vs. 37%). We further tested the reproducibility of the Ti^{4+}-IMAC for phosphoprotein enrichment using the standard protein mixture (BSA:β-casein, 100 μM:10 μM). A reproducible β-casein recovery (48 ± 8%) was produced from quadruplicate preparations. We want to highlight that another important advantage of our Ti^{4+}-IMAC magnetic particles compared to the commercial kit is its easy operations via a magnet without the need for centrifugation. Additionally, the Ti^{4+}-IMAC method could be used for a variety of initial amounts of protein materials via a simple adjustment of the mass of magnetic particles depending on the availability of the biological samples. We noted that there is still a visible BSA band in the eluates of the Ti^{4+}-IMAC (Fig. 3A and C) and there is no clear BSA signal in the elution sample of the commercial kit (Fig. 3B). Some further improvement of the surface chemistry of Ti^{4+}-IMAC magnetic particles could be done to reduce the non-specific binding of non-phosphoproteins and will be investigated in our future study.

Phosphoproteoform enrichment by Ti^{4+}-IMAC nanoparticles and SDS-PAGE analysis: a yeast cell lysate

We further validated the performance of the Ti^{4+}-IMAC magnetic nanoparticles for phosphoproteoform enrichment from a complex sample, a yeast cell lysate. Three milligrams of yeast proteins and 10 mg of Ti^{4+}-IMAC magnetic nanoparticles were used. The experiment was performed in triplicate. We loaded an equal amount of proteins for loading mixture (LM), flow-through (FT), and elution (E) into each lane of SDS-PAGE gel for analysis. We first stained the gel using Pro-Q Diamond to detect phosphoproteoforms

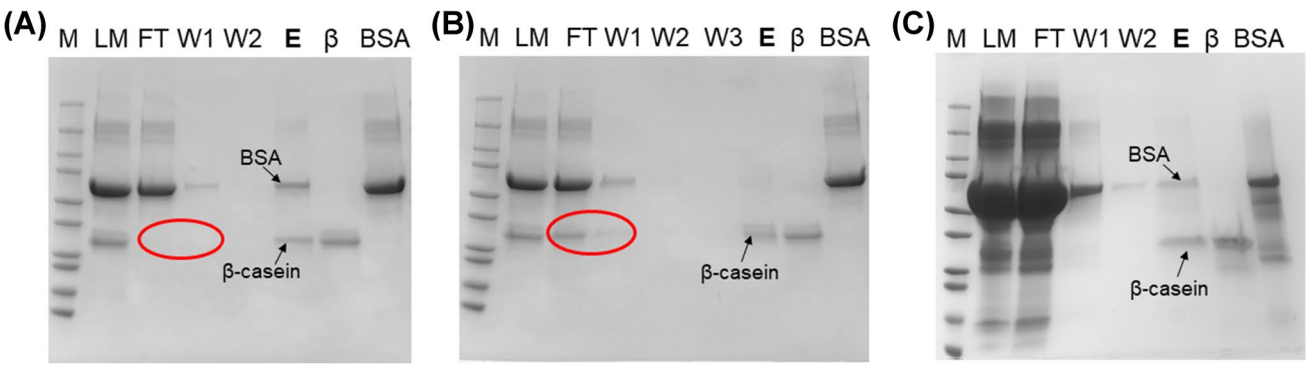

Fig. 3 SDS-PAGE data of a standard protein mixture (BSA and β-casein) after selective isolation of phosphoprotein β-casein with magnetic nanoparticle–based Ti^{4+}-IMAC (**A** and **C**) and the commercial phosphoprotein enrichment kit (**B**). For **A** and **B**, the concentration of BSA and β-casein in the sample was both 10 μM. For **C**, the concentration of BSA was 10 times higher than β-casein (100 μM vs. 10 μM). M, protein molecular weight marker; LM, loading mixture (the standard protein mixture before IMAC enrichment); FT, flow-through; W1, W2, and W3, the first, second, and third wash; E, eluate from the Ti^{4+}-IMAC magnetic nanoparticles after enrichment; β, β-casein standard; BSA, BSA standard

specifically. Then, we de-stained the gel and re-stained it with SYPRO Ruby to detect total proteins in the samples.

As shown in Fig. 4A, much more visible phosphoproteoform bands were observed in the eluates (E1, E2, and E3) compared to the loading mixture (LM) in the triplicate preparations. The Ti^{4+}-IMAC method has nice reproducibility according to the phosphoproteoform profiles in the three eluates (E1, E2, and E3). Figure 4B further shows the nice reproducibility of the technique at the total proteoform level (E1, E2, and E3). By comparing the total proteoform and phosphoproteoform profiles in the eluates, we observed that the major proteoform bands (≤ 75 kDa) are relatively consistent, indicating the reasonably high specificity of the technique for phosphoproteoform enrichment from complex samples. We noted that many visible phosphoproteoform bands exist for the flow-through sample (FT) and some bands even have a higher intensity than that in the eluates (E). To get a better understanding of this phenomenon, we determined the loading capacity of the Ti^{4+}-IMAC nanoparticles using the β-casein as the sample; see Electronic Supplementary Material I Figure S2A. The loading capacity is about 140 μg phosphoproteins/mg nanoparticles for Ti^{4+}-IMAC and the enrichment process could be done within 1 h. The 10 mg of Ti^{4+}-IMAC magnetic nanoparticles used in the experiment could capture more than 1 mg of phosphoproteoforms. Interestingly, only about 200 μg of proteins were recovered in the eluate (E) after the enrichment. The results suggest that the Ti^{4+}-IMAC cannot capture all the phosphoproteoforms in the cell lysate, probably due to the three-dimensional structure of intact phosphoproteoforms and the selectivity of Ti^{4+}.

Considering that IMAC with different metal ions (e.g., Ti^{4+} and Fe^{3+}) could enrich different pools of phosphopeptides from complex proteome samples [39, 40], we compared Ti^{4+}-IMAC and Fe^{3+}-IMAC for phosphoproteoform enrichment for the first time here. The Fe^{3+}-IMAC magnetic nanoparticles were prepared using the same procedure as the Ti^{4+}-IMAC material, and the salt $FeCl_3$ was used as the source of the Fe^{3+}. We employed the same protocol for the phosphoproteoform enrichment from the yeast cell lysate using the Ti^{4+}-IMAC and Fe^{3+}-IMAC magnetic nanoparticles. The loading capacity is about 160 μg phosphoproteins/mg nanoparticles for Fe^{3+}-IMAC nanoparticles; see Electronic Supplementary

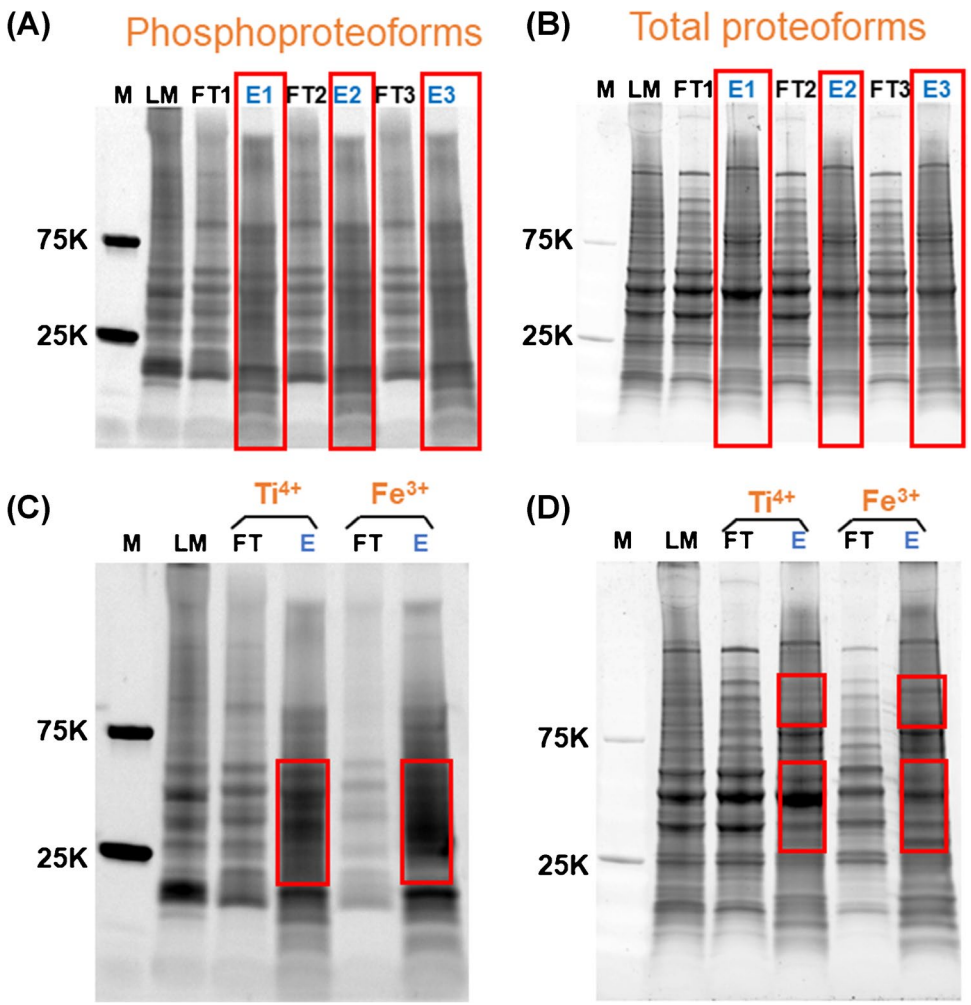

Fig. 4 SDS-PAGE data of a yeast cell lysate. Visualization of phosphoproteoforms by the Pro-Q Diamond staining (**A**) and total proteoforms by SYPRO Ruby staining (**B**) after phosphoproteoform enrichment by magnetic nanoparticle–based Ti^{4+}-IMAC in triplicate experiments. M, protein molecular weight marker; LM, loading mixture (the yeast cell lysate before IMAC enrichment); FT1, FT2, and FT3, flow-through from the first, second, and third experiment; E1, E2, and E3, eluate from the Ti^{4+}-IMAC magnetic nanoparticles after enrichment in the first, second, and third experiment. Direct comparisons of Ti^{4+}-IMAC and Fe^{3+}-IMAC regarding the profile of phosphoproteoforms (**C**) and total proteoforms (**D**) isolated from the yeast cell lysate

Material I Figure S2B. The Ti^{4+}-IMAC and Fe^{3+}-IMAC produced substantially different profiles of phosphoproteoforms, as evidenced by the SDS-PAGE data in Fig. 4C. The total proteoform data in Fig. 4D also indicates the distinguishable differences between Ti^{4+}-IMAC and Fe^{3+}-IMAC eluates. The data indicate that Ti^{4+}-IMAC and Fe^{3+}-IMAC are complementary for phosphoproteoform enrichment from complex proteomes and a combination of the two methods will be useful for improving the phosphoproteoform coverage.

RPLC-MS/MS-based top-down proteomics of yeast phosphoproteoforms enriched by Ti^{4+}-IMAC and Fe^{3+}-IMAC

We further enriched phosphoproteoforms from the yeast cell lysate using both Ti^{4+}-IMAC and Fe^{3+}-IMAC and analyzed the loading mixture (LM) and eluates (E) by RPLC-MS/MS. After database search by the TopPIC, 15, 28, and 32 phosphoproteoforms were identified from the LM, E of Ti^{4+}-IMAC, and E of Fe^{3+}-IMAC, respectively, with a 5% proteoform-level FDR. The identified phosphoproteoforms and total proteoforms are listed in the Electronic Supplementary Material II.

The IMAC technique yielded about 100% more phosphoproteoform identifications compared to a direct RPLC-MS/MS analysis of the LM without enrichment (about 30 vs. 15). Interestingly, Ti^{4+}-IMAC and Fe^{3+}-IMAC produced obviously different phosphoproteoform profiles, evidenced by the low proteoform-level overlap between the two methods (Fig. 5A). In total, 48 phosphoproteoforms were identified by the two IMAC methods and only 12 of them were identified by both methods. The data agree well with the data in Fig. 4C. We noted that only 3 out of 15 phosphoproteoforms identified in the LM sample were also identified in the E of Ti^{4+}-IMAC or Fe^{3+}-IMAC, indicating that some phosphoproteoforms cannot be captured by the IMAC materials during the enrichment step, which agrees well with the SDS-PAGE data in Fig. 4.

We speculated that proteins corresponding to the phosphoproteoforms identified in the LM had a relatively high abundance in the yeast cells, and the phosphoproteoforms can be identified directly by RPLC-MS/MS without the need for IMAC enrichment. However, for the phosphoproteoforms identified in the E after Ti^{4+}-IMAC or Fe^{3+}-IMAC, the corresponding proteins have relatively low abundance in the yeast cells and IMAC enrichment is critical for the characterization of those phosphoproteoforms. To prove this hypothesis, we first checked the protein-level overlaps among LM, E of Ti^{4+}-IMAC, and E of Fe^{3+}-IMAC for the identified phosphoproteoforms, followed by the investigation of protein relative abundance according to the Protein Abundance Database (PAXdb, version 4.2, https://pax-db.org/species/4932). As shown in Fig. 5B, the protein-level overlaps between LM and E of Ti^{4+}-IMAC or LM and E of Fe^{3+}-IMAC are low. The protein abundance data in Fig. 5C clearly indicate that phosphoproteins identified in the Es after IMAC enrichment have much lower abundance compared to that identified in the LM. The data clearly demonstrate the benefits of Ti^{4+}-IMAC and Fe^{3+}-IMAC enrichment for top-down proteomics of phosphoproteoforms with low abundance.

We noted that the number of phosphoproteoforms identified from IMAC eluates here is small compared to the total number of proteoform identifications (~30 vs. ~600). Those about 600 proteoforms correspond to roughly 200 proteins and the approximate 30 phosphoproteoforms derive from about 10 proteins. We further manually checked the identified total proteins from the Ti^{4+}-IMAC and Fe^{3+}-IMAC eluates in terms of phosphorylation through the online protein phosphorylation database PhosphoGRID (https://phosphogrid.org/). We found that at least more than 50% of those proteins have been reported as phosphorylated proteins. The reason why we only identified roughly 30 phosphoproteoforms of 10 proteins from each of the IMAC eluates by RPLC-MS/MS might be due to the phosphate group loss during sample processing and storage before RPLC-MS/MS. During the proteoform elution, buffer exchange, and sample

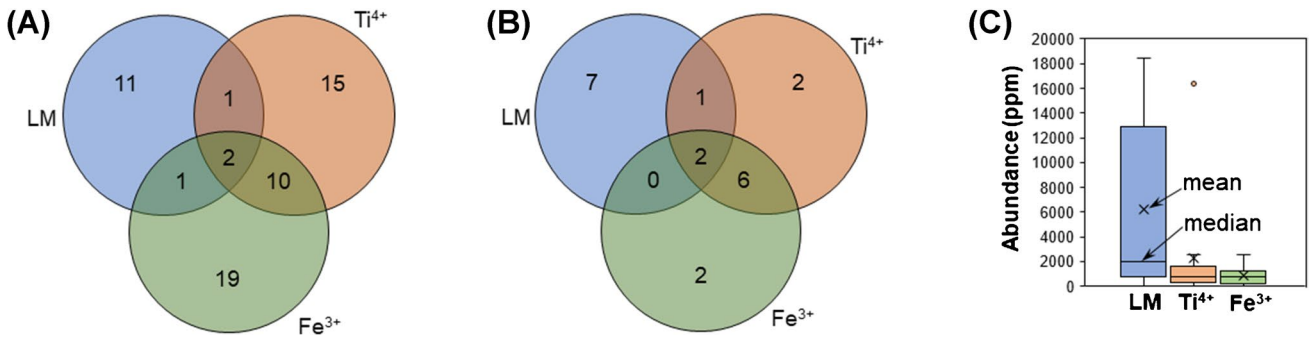

Fig. 5 Phosphoproteoform identification results from the yeast cell lysate by RPLC-MS/MS. **A** Proteoform-level overlap among phosphoproteoforms identified from the yeast sample before IMAC enrichment (loading mixture, LM), after Ti^{4+}-IMAC enrichment (Ti^{4+}), and after Fe^{3+}-IMAC enrichment (Fe^{3+}). **B** Protein-level overlap among LM, Ti^{4+}, and Fe^{3+} for the identified phosphoproteoforms. **C** Boxplots of abundance (ppm) of proteins corresponding to the identified phosphoproteoforms from LM, Ti^{4+}, and Fe.$^{3+}$. The protein abundance information was obtained from the Protein Abundance Database (PAXdb, version 4.2, https://pax-db.org/species/4932)

storage steps, the phosphate groups could be lost due to potential phosphatase activity because phosphatase inhibitors most likely have been removed. However, it is hard to make a solid conclusion about this point here. We will study the sample processing procedure in more detail and more samples to achieve a better understanding of this phenomenon in our future work.

Figure 6 shows two examples of identified phosphoproteoforms from the yeast cell lysate by Ti^{4+}-IMAC or Fe^{3+}-IMAC enrichment and RPLC-MS/MS. One phosphoproteoform of gene *HYP2* (eukaryotic translation initiation factor 5A-1) shows a strong signal after Ti^{4+}-IMAC enrichment, but without a visible signal before enrichment (Fig. 6A). In another example shown in Fig. 6B, one phosphoproteoform of gene *STF2* (ATPase-stabilizing factor 15 kDa protein) has drastically better signal after Fe^{3+}-IMAC enrichment compared to before enrichment. The data further demonstrate the highly efficient phosphoproteoform enrichment from complex samples by the Ti^{4+}-IMAC and Fe^{3+}-IMAC. Interestingly, we detected clear signals of the corresponding un-phosphoproteoforms of the genes *HYP2* and *STF2* not only before enrichment but also after IMAC enrichment, which might be due to either the dynamic nature of protein phosphorylation (loss of phosphate groups during the steps after enrichment) or the non-specific binding of un-phosphoproteoforms on the IMAC magnetic nanoparticles. Figure 6C and D show the sequences and fragmentation patterns of two identified phosphoproteoforms. The two phosphoproteoforms were identified with high confidence and were characterized reasonably well. We noted that the proteoform shown in Fig. 6C has both acetylation and phosphorylation close to its N-terminus. Although the database search software assigned the acetylation to the S2 residue and the phosphorylation to the S8 residue, there are still uncertainties in the PTM localization because of the lack of fragment ions from the first 10 amino acid residues. The data indicate a general challenge in top-down proteomics for accurate PTM localization.

Figure S3 in Electronic Supplementary Material I shows the sequences and fragmentation patterns of four example phosphoproteoforms with the combinations of multiple PTMs. Three phosphoproteoforms of eukaryotic translation initiation factor 5A-1 (IF5A1) were identified with two phosphorylation sites (A), combinations of phosphorylation, hypusination, and acetylation (B), and combinations of phosphorylation, hypusination, and truncation (C). We identified over 10 different phosphopoteoforms of IF5A1 by Ti^{4+}-IMAC and

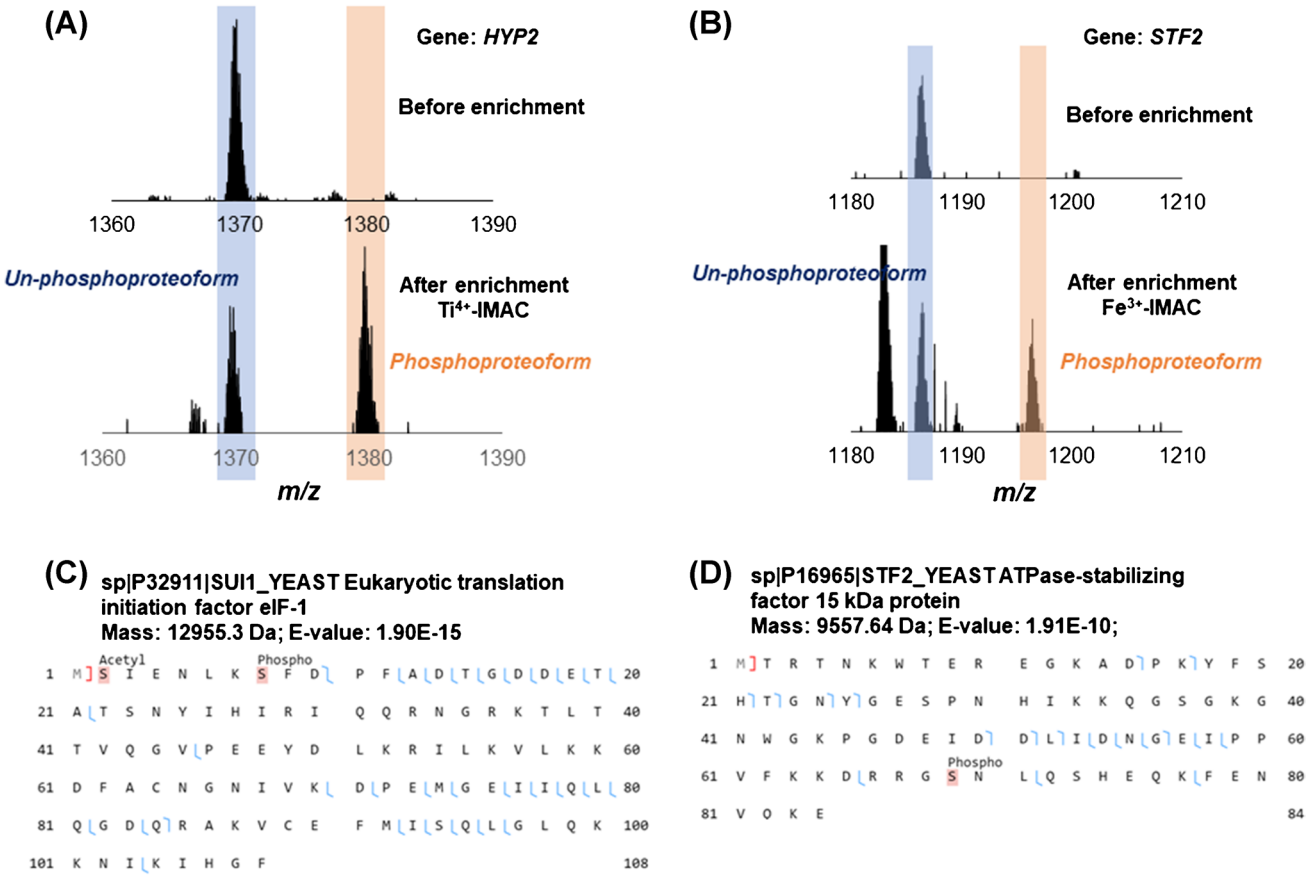

Fig. 6 **A** Mass spectra of one HYP2 phosphoproteoform before and after Ti^{4+}-IMAC enrichment. **B** Mass spectra of one STF2 phosphoproteoform before and after Fe^{3+}-IMAC enrichment. **C**, **D** Sequences and fragmentation patterns of two example phosphoproteoforms

Fe^{3+}-IMAC enrichment, suggesting the huge potential heterogeneity of phosphoproteoforms from the same gene. It is impossible to reveal the proteoform-level heterogeneity using the traditional BUP strategy. IF5A is a translation factor, and it has crucial functions in modulating cancer and brain aging [41, 42]. However, the detailed functions of IF5A phosphorylation and hypusination in those processes are not clear. The capability of delineating various IF5A phosphoproteoforms with or without hypusination using TDP will establish the foundation for further elucidating their functions in cancer and brain aging. The data here highlight the significance of TDP for protein characterization in a proteoform-specific manner.

Conclusions

In this pilot study, we investigated magnetic nanoparticle–based IMAC (Ti^{4+} and Fe^{3+}) for the enrichment of phosphoproteoforms from simple and complex protein mixtures for MS-based top-down proteomics. The IMAC methods achieved highly efficient and reproducible enrichment of intact phosphoproteoforms from a standard protein mixture and a yeast cell lysate. Substantially more phosphoproteoforms were identified from the yeast cell lysate after IMAC enrichment with Ti^{4+} or Fe^{3+} compared to that without enrichment. Interestingly, we documented that Ti^{4+}-IMAC and Fe^{3+}-IMAC tended to isolate different pools of phosphoproteoforms from a complex proteome.

We note that some improvements need to be made to achieve global top-down proteomics of phosphoproteoforms from complex proteomes. First, the surface chemistry of Ti^{4+} and Fe^{3+}-IMAC magnetic particles could be improved to reduce the non-specific binding of non-phosphoproteins and further boost the phosphoproteoform recovery. Second, the mass of all the identified phosphoproteoforms by RPLC-MS/MS is smaller than 20 kDa in this work due to the low sensitivity of top-down proteomics for the characterization of large proteoforms. Improvement of MS-based top-down proteomics technique for the identification of large phosphoproteoforms will be an important topic in our future studies. Third, the full characterization of phosphoproteoforms is hampered by the unsatisfying backbone cleavage coverage of proteoforms from the typical LC–MS/MS technique with collision-based gas-phase fragmentation. We expect that coupling our IMAC techniques to LC–MS/MS equipped with collision, electron, and photon-based gas-phase fragmentation methods will advance the top-down proteomics of phosphoproteoforms drastically.

Supplementary Information The online version contains supplementary material available at https://doi.org/10.1007/s00216-023-04677-9.

Funding We received the support from National Cancer Institute through Grant R01CA247863. We also received the support from the National Institute of General Medical Sciences (NIGMS) through Grants 2R01GM118470 and R01GM125991 and the National Science Foundation through Grant DBI1846913 (CAREER Award).

Declarations

Conflict of interest The authors declare no competing interests.

References

1. Graves JD, Krebs EG. Protein phosphorylation and signal transduction. Pharmacol Ther. 1999;82:111–21. https://doi.org/10.1016/s0163-7258(98)00056-4.
2. Pawson T, Scott JD. Protein phosphorylation in signaling--50 years and counting. Trends Biochem Sci. 2005;30:286–90. https://doi.org/10.1016/j.tibs.2005.04.013.
3. Tarrant MK, Cole PA. The chemical biology of protein phosphorylation. Annu Rev Biochem. 2009;78:797–825. https://doi.org/10.1146/annurev.biochem.78.070907.103047.
4. Lemeer S, Heck AJR. The phosphoproteomics data explosion. Curr Opin Chem Biol. 2009;13:414–20. https://doi.org/10.1016/j.cbpa.2009.06.022.
5. Ardito F, Giuliani M, Perrone D, Troiano G, Lo ML. The crucial role of protein phosphorylation in cell signaling and its use as targeted therapy (Review). Int J Mol Med. 2017;40:271–80. https://doi.org/10.3892/ijmm.2017.3036.
6. Wang F, Song C, Cheng K, Jiang X, Ye M, Zou H. Perspectives of comprehensive phosphoproteome analysis using shotgun strategy. Anal Chem. 2011;83:8078–85. https://doi.org/10.1021/ac201833j.
7. Smith LM, Kelleher NL. Proteoform: a single term describing protein complexity. Nat Methods. 2013;10:186–7. https://doi.org/10.1038/nmeth.2369.
8. Yang X, Coulombe-Huntington J, Kang S, Sheynkman GM, Hao T, Richardson A, Sun S, Yang F, Shen YA, Murray RR, Spirohn K, Begg BE, Duran-Frigola M, MacWilliams A, Pevzner SJ, Zhong Q, Trigg SA, Tam S, Ghamsari L, Sahni N, Yi S, Rodriguez MD, Balcha D, Tan G, Costanzo M, Andrews B, Boone C, Zhou XJ, Salehi-Ashtiani K, Charloteaux B, Chen AA, Calderwood MA, Aloy P, Roth FP, Hill DE, Iakoucheva LM, Xia Y, Vidal M. Widespread expansion of protein interaction capabilities by alternative splicing. Cell. 2016;164:805–17. https://doi.org/10.1016/j.cell.2016.01.029.
9. Smith LM, Agar JN, Chamot-Rooke J, Danis PO, Ge Y, Loo JA, Paša-Tolić L, Tsybin YO, Kelleher NL. The Human Proteoform Project: defining the human proteome. Sci Adv. 2021;7:eabk0734. https://doi.org/10.1126/sciadv.abk0734.
10. Smith LM, Kelleher NL. Proteoforms as the next proteomics currency. Science. 2018;359:1106–7. https://doi.org/10.1126/science.aat1884.
11. Wang T, Holt MV, Young NL. The histone H4 proteoform dynamics in response to SUV4-20 inhibition reveals single molecule mechanisms of inhibitor resistance. Epigenetics Chromatin. 2018;11:29. https://doi.org/10.1186/s13072-018-0198-9.
12. Tucholski T, Cai W, Gregorich ZR, Bayne EF, Mitchell SD, McIlwain SJ, de Lange WJ, Wrobbel M, Karp H, Hite Z, Vikhorev PG, Marston SB, Lal S, Li A, Dos Remedios C, Kohmoto T, Hermsen J, Ralphe JC, Kamp TJ, Moss RL, Ge Y. Distinct hypertrophic cardiomyopathy genotypes result in convergent sarcomeric proteoform profiles revealed by top-down proteomics. Proc Natl Acad Sci U S A. 2020;117:24691–700. https://doi.org/10.1073/pnas.2006764117.
13. Toby TK, Fornelli L, Kelleher NL. Progress in top-down proteomics and the analysis of proteoforms. Annu Rev Anal Chem (Palo Alto Calif). 2016;9:499–519. https://doi.org/10.1146/annurev-anchem-071015-041550.
14. Chen B, Brown KA, Lin Z, Ge Y. Top-down proteomics: ready for prime time? Anal Chem. 2018;90:110–27. https://doi.org/10.1021/acs.analchem.7b04747.
15. Wang Q, Sun L, Lundquist PK. Large-scale top-down proteomics of the Arabidopsis thaliana leaf and chloroplast proteomes. Proteomics. 2022; e2100377. https://doi.org/10.1002/pmic.202100377.

16. Ansong C, Wu S, Meng D, Liu X, Brewer HM, Deatherage Kaiser BL, Nakayasu ES, Cort JR, Pevzner P, Smith RD, Heffron F, Adkins JN, Pasa-Tolic L. Top-down proteomics reveals a unique protein S-thiolation switch in Salmonella Typhimurium in response to infection-like conditions. Proc Natl Acad Sci U S A. 2013;110:10153–8. https://doi.org/10.1073/pnas.1221210110.
17. Ntai I, Fornelli L, DeHart CJ, Hutton JE, Doubleday PF, LeDuc RD, van Nispen AJ, Fellers RT, Whiteley G, Boja ES, Rodriguez H, Kelleher NL. Precise characterization of KRAS4b proteoforms in human colorectal cells and tumors reveals mutation/modification cross-talk. Proc Natl Acad Sci U S A. 2018;115:4140–5. https://doi.org/10.1073/pnas.1716122115.
18. Melani RD, Gerbasi VR, Anderson LC, Sikora JW, Toby TK, Hutton JE, Butcher DS, Negrão F, Seckler HS, Srzentić K, Fornelli L, Camarillo JM, LeDuc RD, Cesnik AJ, Lundberg E, Greer JB, Fellers RT, Robey MT, DeHart CJ, Forte E, Hendrickson CL, Abbatiello SE, Thomas PM, Kokaji AI, Levitsky J, Kelleher NL. The Blood Proteoform Atlas: a reference map of proteoforms in human hematopoietic cells. Science. 2022;375:411–8. https://doi.org/10.1126/science.aaz5284.
19. Tran JC, Zamdborg L, Ahlf DR, Lee JE, Catherman AD, Durbin KR, Tipton JD, Vellaichamy A, Kellie JF, Li M, Wu C, Sweet SMM, Early BP, Siuti N, LeDuc RD, Compton PD, Thomas PM, Kelleher NL. Mapping intact protein isoforms in discovery mode using top-down proteomics. Nature. 2011;480:254–8. https://doi.org/10.1038/nature10575.
20. Villen J, Gygi SP. The SCX/IMAC enrichment approach for global phosphorylation analysis by mass spectrometry. Nat Protoc. 2008;3:1630–8. https://doi.org/10.1038/nprot.2008.150.
21. Zhou H, Ye M, Dong J, Han G, Jiang X, Wu R, Zou H. Specific phosphopeptide enrichment with immobilized titanium ion affinity chromatography adsorbent for phosphoproteome analysis. J Proteome Res. 2008;7:3957–67. https://doi.org/10.1021/pr800223m.
22. Gruhler A, Olsen JV, Mohammed S, Mortensen P, Faergeman NJ, Mann M, Jensen ON. Quantitative phosphoproteomics applied to the yeast pheromone signaling pathway. Mol Cell Proteomics. 2005;4:310–27. https://doi.org/10.1074/mcp.M400219-MCP200.
23. Andersson L, Porath J. Isolation of phosphoproteins by immobilized metal (Fe3+) affinity chromatography. Anal Biochem. 1986;154:250–4. https://doi.org/10.1016/0003-2697(86)90523-3.
24. Steen H, Kuster B, Fernandez M, Pandey A, Mann M. Tyrosine phosphorylation mapping of the epidermal growth factor receptor signaling pathway. J Biol Chem. 2002;277:1031–9. https://doi.org/10.1074/jbc.M109992200.
25. Grønborg M, Kristiansen TZ, Stensballe A, Andersen JS, Ohara O, Mann M, Jensen ON, Pandey A. A mass spectrometry-based proteomic approach for identification of serine/threonine-phosphorylated proteins by enrichment with phospho-specific antibodies: identification of a novel protein, Frigg, as a protein kinase A substrate. Mol Cell Proteomics. 2002;1:517–27. https://doi.org/10.1074/mcp.m200010-mcp200.
26. Pandey A, Podtelejnikov AV, Blagoev B, Bustelo XR, Mann M, Lodish HF. Analysis of receptor signaling pathways by mass spectrometry: identification of vav-2 as a substrate of the epidermal and platelet-derived growth factor receptors. Proc Natl Acad Sci U S A. 2000;97:179–84. https://doi.org/10.1073/pnas.97.1.179.
27. Schmidt SR, Schweikart F, Andersson ME. Current methods for phosphoprotein isolation and enrichment. J Chromatogr B. 2007;849:154–62. https://doi.org/10.1016/j.jchromb.2006.09.016.
28. Alpert AJ, Hudecz O, Mechtler K. Anion-exchange chromatography of phosphopeptides: weak anion exchange versus strong anion exchange and anion-exchange chromatography versus electrostatic repulsion-hydrophilic interaction chromatography. Anal Chem. 2015;87:4704–11. https://doi.org/10.1021/ac504420c.
29. Li Y, Wang Y, Dong M, Zou H, Ye M. Sensitive approaches for the assay of the global protein tyrosine phosphorylation in complex samples using a mutated SH2 domain. Anal Chem. 2017;89:2304–11. https://doi.org/10.1021/acs.analchem.6b03812.
30. Bian Y, Li L, Dong M, Liu X, Kaneko T, Cheng K, Liu H, Voss C, Cao X, Wang Y, Litchfield D, Ye M, Li SS-C, Zou H. Ultra-deep tyrosine phosphoproteomics enabled by a phosphotyrosine superbinder. Nat Chem Biol. 2016;12:959–66. https://doi.org/10.1038/nchembio.2178.
31. Hwang L, Ayaz-Guner S, Gregorich ZR, Cai W, Valeja SG, Jin S, Ge Y. Specific enrichment of phosphoproteins using functionalized multivalent nanoparticles. J Am Chem Soc. 2015;137:2432–5. https://doi.org/10.1021/ja511833y.
32. Roberts DS, Chen B, Tiambeng TN, Wu Z, Ge Y, Jin S. Reproducible large-scale synthesis of surface silanized nanoparticles as an enabling nanoproteomics platform: enrichment of the human heart phosphoproteome. Nano Res. 2019;12:1473–81. https://doi.org/10.1007/s12274-019-2418-4.
33. Chen B, Hwang L, Ochowicz W, Lin Z, Guardado-Alvarez TM, Cai W, Xiu L, Dani K, Colah C, Jin S, Ge Y. Coupling functionalized cobalt ferrite nanoparticle enrichment with online LC/MS/MS for top-down phosphoproteomics. Chem Sci. 2017;8:4306–11. https://doi.org/10.1039/c6sc05435h.
34. Wang M-M, Chen S, Yu Y-L, Wang J-H. Novel Ti(4+)-chelated polyoxometalate/polydopamine composite microspheres for highly selective isolation and enrichment of phosphoproteins. ACS Appl Mater Interfaces. 2019;11:37471–8. https://doi.org/10.1021/acsami.9b12872.
35. Kou Q, Xun L, Liu X. TopPIC: a software tool for top-down mass spectrometry-based proteoform identification and characterization. Bioinformatics. 2016;32:3495–7. https://doi.org/10.1093/bioinformatics/btw398.
36. Kessner D, Chambers M, Burke R, Agus D, Mallick P. ProteoWizard: open source software for rapid proteomics tools development. Bioinformatics. 2008;24:2534–6. https://doi.org/10.1093/bioinformatics/btn323.
37. Keller A, Nesvizhskii AI, Kolker E, Aebersold R. Empirical statistical model to estimate the accuracy of peptide identifications made by MS/MS and database search. Anal Chem. 2002;74:5383–92. https://doi.org/10.1021/ac025747h.
38. Elias JE, Gygi SP. Target-decoy search strategy for increased confidence in large-scale protein identifications by mass spectrometry. Nat Methods. 2007;4:207–14. https://doi.org/10.1038/nmeth1019.
39. Yue X, Schunter A, Hummon AB. Comparing multistep immobilized metal affinity chromatography and multistep TiO2 methods for phosphopeptide enrichment. Anal Chem. 2015;87:8837–44. https://doi.org/10.1021/acs.analchem.5b01833.
40. Tsai C-F, Hsu C-C, Hung J-N, Wang Y-T, Choong W-K, Zeng M-Y, Lin P-Y, Hong R-W, Sung T-Y, Chen Y-J. Sequential phosphoproteomic enrichment through complementary metal-directed immobilized metal ion affinity chromatography. Anal Chem. 2014;86:685–93. https://doi.org/10.1021/ac4031175.
41. Mathews MB, Hershey JWB. The translation factor eIF5A and human cancer. Biochim Biophys Acta. 2015;1849:836–44. https://doi.org/10.1016/j.bbagrm.2015.05.002.
42. Liang Y, Piao C, Beuschel CB, Toppe D, Kollipara L, Bogdanow B, Maglione M, Lützkendorf J, See JCK, Huang S, Conrad TOF, Kintscher U, Madeo F, Liu F, Sickmann A, Sigrist SJ. eIF5A hypusination, boosted by dietary spermidine, protects from premature brain aging and mitochondrial dysfunction. Cell Rep. 2021;35:108941. https://doi.org/10.1016/j.celrep.2021.108941.